Lessons Learned from Operating an On-site Earthquake Early Warning System

A.Zaicenco
Terrascience Systems Ltd., Vancouver, BC, Canada

I.Weir-Jones
Weir-Jones Engineering Ltd., Vancouver, BC, Canada

SUMMARY:
Earthquake Early Warning Systems (EEWS) represent a modern seismic risk reduction tool. They allow for emergency shutdown of critical facilities susceptible to damage due to excessive dynamic loads. The on-site system in the Vancouver area, British Columbia, uses individual sensors and performs site observation with the goal to identify the P-wave associated with a target seismic event. High cost of the down-time of the critical infrastructure imposes the following demands on the EEWS: high reliability of the continuous autonomous operation, inadmissibility of false alarms, access to the system over the Internet, and availability of a comprehensive maintenance plan. In this paper, we describe the lessons learned from designing, installing and using an on-site EEWS, which has been successfully operating since mid-2009. We address several major problems related to: system configuration, P-wave identification algorithm, and interpretation of the collected data.

Keywords: earthquake early warning system, risk reduction, real-time instrumentation

1. INTRODUCTION

Design of an on-site EEWS for critical facilities based on P-wave detection, requires knowledge of local seismicity, local geological settings, and potential soil-structure interaction effects (Zaicenco et al. 2010). The scope of the current paper is to present an efficient and reliable methodology used for P-wave detection and discrimination using multiple parameters. It is tolerant to the environmental, traffic and other types of noise at the location of the critical facility.

A system consisting of borehole sensor array that has been designed based on these ideas is described and records of several regional earthquakes are provided. This system was implemented in 2009 to provide earthquake early warning for a tunnel on a major highway in British Columbia, Canada. Since mission-critical systems are evaluated via risk analysis, we specify the required reliability of the EEWS components in such a way that it meets operational goals for the warning system lifetime. Reliability of the P-wave detection algorithm is achieved via multiple redundancies, which decreases the probability of a false alarm.

Since on-site EEWS is continuously collecting data over an extensive period of time, we emphasize the dual use of the system as a tool to provide early warning, and a tool to improve the local seismic hazard information and its site-specific manifestations. We include several examples of the regional earthquake records, which not only confirmed the P-wave detection method, but also allowed us to quantify the local geological conditions at the site and parameterize the seismic loads experienced by the critical facility.

Lessons learned from operating the on-site EEWS represent a valuable experience in view of the "Hyogo Framework for Action 2005-2015" adopted by the UN International Strategy for Disaster Reduction, which specified monitoring disaster risks and enhancing early warning as one of its priorities for action.

2. SEISMIC HAZARD IN SW BRITISH COLUMBIA

The Cascadia subduction zone stretches from the Brooks Peninsula on Vancouver Island in the north to Cape Mendocino in California in the south, and is lying on the contact between the Juan de Fuca

Plate and the North American Plate off Pacific coast. The Juan de Fuca plate is diverging from the Pacific plate with the rate 2.9-3.1 cm/yr (Atwater 1970), and subducting at a rate 4.5 cm/yr against the North American Plate (Riddihough 1984). The sea floor subducts under the North American plate and shapes the Cascade Range in British Columbia, Washington, Oregon and the Northern California. The angle of subduction is ≈17° beneath Vancouver Island (Hyndman et al. 1990). The seismic hazard in this region, Fig. 1(a), is represented by three major sources:

(a) Shallow/crustal earthquakes with magnitude M<7.5. These are large in numbers, and attenuation of PGA with distance is strong. The largest crustal earthquake occurred in 1946 on Vancouver Island and had magnitude Ms=7.3.

(b) Intraplate earthquakes with focal depth > 30 km and magnitude M<7. They occur on fractures of Juan de Fuca plate and are concentrated along the west coast of Vancouver Island and beneath Puget Sound (Balfour 2011). Attenuation law is less pronounced with epicentral distance.

(c) Subduction zone/megathrust earthquakes, which can reach M≈9. Large events occur with the interval 200-1000yrs (Goldfinger et al. 2008), and long-period frequency content is characterizing the source spectrum.

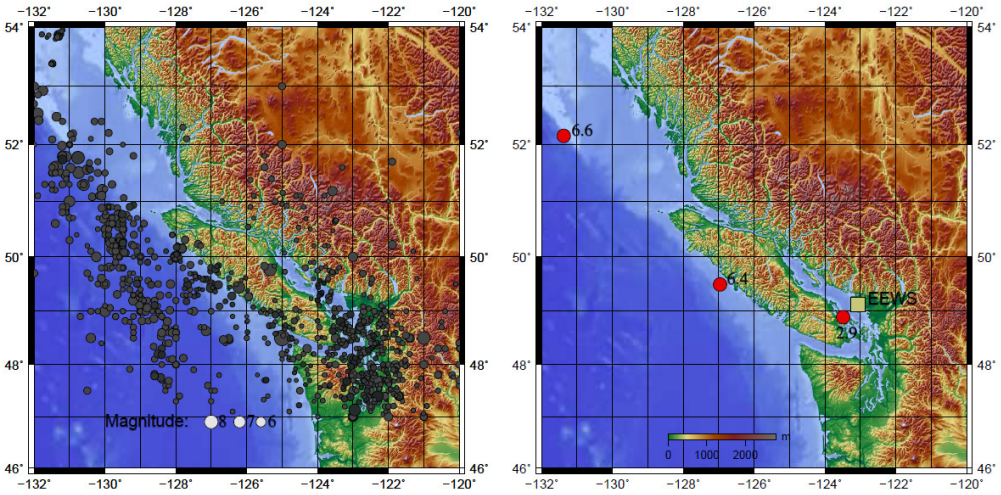

(a) (b)

Figure 1. (a) Historical earthquakes in SW British Columbia, (b) several significant seismic events recorded by the EEWS during 2009-2011 (2009/11/17 M=6.6, 2011/02/15 M=2.9, 2011/09/09 M=6.4)

In general, seismicity in British Columbia does not relate to the surface expression of faults (Rogers 1998). Random character of crustal earthquakes was studied by (Cassidy et al. 2000) who identified lineations and some active structures. As pointed out in (Balfour 2011), investigating SW British Columbia using the World Stress Map shows no formal stress inversions and only a few single focal mechanisms. The same author inverted focal mechanisms to determine the stress orientation and regime.

According to the GSHAP seismic hazard map, the SW part of British Columbia is included into the zone with PGA≈1.6-2.4m/s2 with 10% probability of exceedance in 50 years. In the greater Vancouver area thick and soft sediments of the Fraser River delta have the potential to modify the amplitude-frequency content of the seismic waves. The fine-grained alluvial sediments are up to about 300 m thick and are mainly silts and clays (Cassidy and Rogers 1999). Share-wave velocities in these sediments are, on average, 200 m/s, and are about 100 m/s near the surface. Strong-motion recordings of 1996 Duvall and 1997 Georgia Strait earthquakes allowed to perform site response studies in the greater Vancouver area (Cassidy and Rogers 1999), which revealed amplification on the Fraser River delta of 2-6 times relative to firm soil sites and peak amplification around 1-3 Hz.

3. PECULIARITIES OF THE ON-SITE EEWS

EEWS based on the measurements of the first P-wave arrivals are generally considered as either regional (network-based) or on-site (stand-alone) systems (Kanamori 2005), and their aim is to provide a rapid notification of the potential damaging effects of the impeding earthquake. For the on-site system the alert is issued based on the local measurements of the P-wave ground motion (Zollo et al. 2010). The on-site systems are designed to protect an individual critical facility and cover a very limited geographic area (Saita et al. 2008).

EEWS can be a useful tool in seismic hazard reduction if the spatial relation between cities and earthquake sources is favorable for such warning (Wu and Kanamori 2008). The warning time, based on P-S traveltime difference can measure from zero, when the epicenter is too close to the site, to up to dozen of seconds, when the epicenter is located hundreds of kilometers away from the site, but still generates a dangerous ground motion.

Several factors represented the main challenge in designing the on-site EEWS that protects a critical facility in the Vancouver area:

(a) Unknown direction of a potential seismic event, since sources that are capable of generating the ground motion that exceeds design parameters are spread around the region, Fig. 1(a);
(b) Multiple sources of industrial noise at the site: highway traffic, railroad, fishery, heavy trucks driving several meters away from the instrumented area;
(c) Requirement for the system to operate 24/7 in the autonomous mode for several years;
(d) High cost of a potential false alarm, which might result in closing the traffic on the major highway.

4. P-WAVE DETECTION USING TRIAXIAL SENSORS

The equation of the seismic wave propagation in the elastic medium under assumption that Lame parameters λ and μ are constant is:

$$\rho\ddot{\mathbf{u}} = (\lambda + 2\mu)\nabla(\nabla \cdot \mathbf{u}) - \mu\nabla \times (\nabla \times \mathbf{u}) \tag{4.1}$$

where ρ is the density of material and $\mathbf{u}$ is the displacement vector. This is a 3D homogeneous vector wave equation for a uniform, isotropic linear medium. In a general case, the medium is anisotropic and inhomogeneous, but for the sake of simplicity we will focus on the equation for the homogeneous medium given above.

Applying Helmholtz theorem to this equation (i.e. a curl-free Φ, and divergence-free Θ, fields describe the total displacement vector field) and simplifying it, we obtain two wave equations: one for scalar potential and one for vector potential:

$$\frac{(\lambda+2\mu)}{\rho}\frac{\partial^2\Phi}{\partial t^2} = \frac{(\lambda+2\mu)}{\rho}\nabla^2\Phi \quad \text{and} \quad \frac{\partial^2\Theta}{\partial t^2} = \frac{\mu}{\rho}\nabla^2\Theta \tag{4.2}$$

The speeds at which these waves propagate are:

$$V_P^2 = \frac{\lambda+2\mu}{\rho} \quad \text{and} \quad V_S^2 = \frac{\mu}{\rho} \tag{4.3}$$

Fig. 2 illustrates elastic wave propagation in a 2D homogeneous medium from a point source with the formation of P and S waves. The volumetric change associated with dilatation terms of the strain tensor:

$$\nabla \mathbf{u} = \frac{\partial u_1}{\partial x_1} + \frac{\partial u_2}{\partial x_2} + \frac{\partial u_3}{\partial x_3} \tag{4.4}$$

is related to P waves. And shear distortion related to S waves is described by the off-diagonal terms of the strain tensor:

$$\varepsilon_{ij} = \frac{1}{2}\left(\frac{\partial u_i}{\partial x_j} + \frac{\partial u_j}{\partial x_i} \right) \tag{4.5}$$

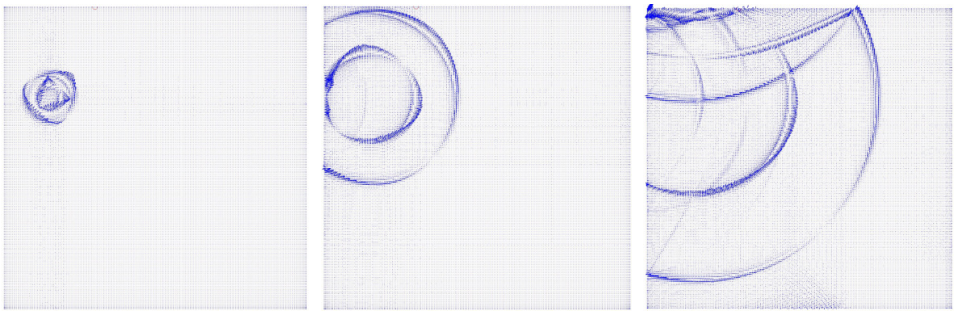

Figure 2. Example of a 2D elastic wave propagation in the homogeneous medium (Zaicenco and Alkaz 2008)

A triaxial sensor is not capable of recovering the components of a strain tensor ε_{ij} to discriminate between P and S waves, but can capture the polarization properties of a 3D particle motion produced by these waves, Fig. 3. This is used as an additional criterion for phase separation and seismic source characterization (Zaicenco and Weir-Jones 2011).

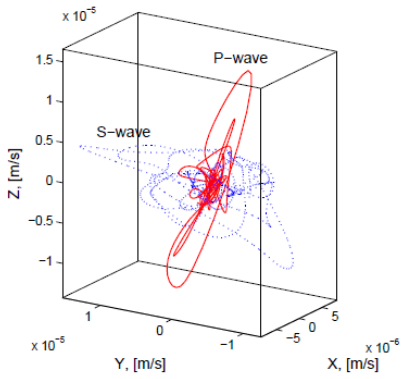

Figure 3. Polarized P- (red line) and S-wave (dashed blue line) phases obtained from a triaxial record, (Zaicenco and Weir-Jones 2011)

5. INPUT INFORMATION FOR EEWS DESIGN

The limit state for the on-site EEWS located on a major highway near Vancouver, British Columbia, is defined by the liquefaction potential of the alluvial deposits when large pore pressure values will likely trigger this undesired phenomenon. Using SHAKE program analysis (Seed et al. 1992), the cyclic stress ratio induced by a scenario earthquake has been compared with the liquefaction resistance and corresponding threshold levels of PGA were computed. They correspond to the mean return period T≈175 yrs, which generate PGA≈0.13g.

Valuable input information represented a set of ground motion records from Nisqually intraslab M=6.8, h=52 km earthquake occurred 17 km NW from Olympia, WA on February 28, 2001. Ground motions were recorded by a set of accelerometers operated by the University of British Columbia at the site where the critical facility is located (Onur et al. 2001), which was 218 km away from the epicenter. Response spectra and H/V ratios of the recorded earthquake are provided in Fig. 4. These spectra demonstrate the presence of long-period components due to local thick sedimentary soft soil conditions and effects of the soil-structure interaction.

A set of Nisqually earthquake records was also provided for the preliminary study by the Pacific Geoscience Center. The seismic station KID in the region of Fraser River delta demonstrated the presence of higher frequency components in the P phase in comparison with the S phase. Polarization analysis of P- and S-phase of the record showed orthogonality of these components and in-plane polarization of the S-wave, which was used as an important discrimination characteristic for design of the EEWS.

Reports with the detailed geotechnical cross-sections of the site were made available by the Ministry of Transport, British Columbia. These reports also contained information about the liquefaction analysis and CPT measurements from several boreholes.

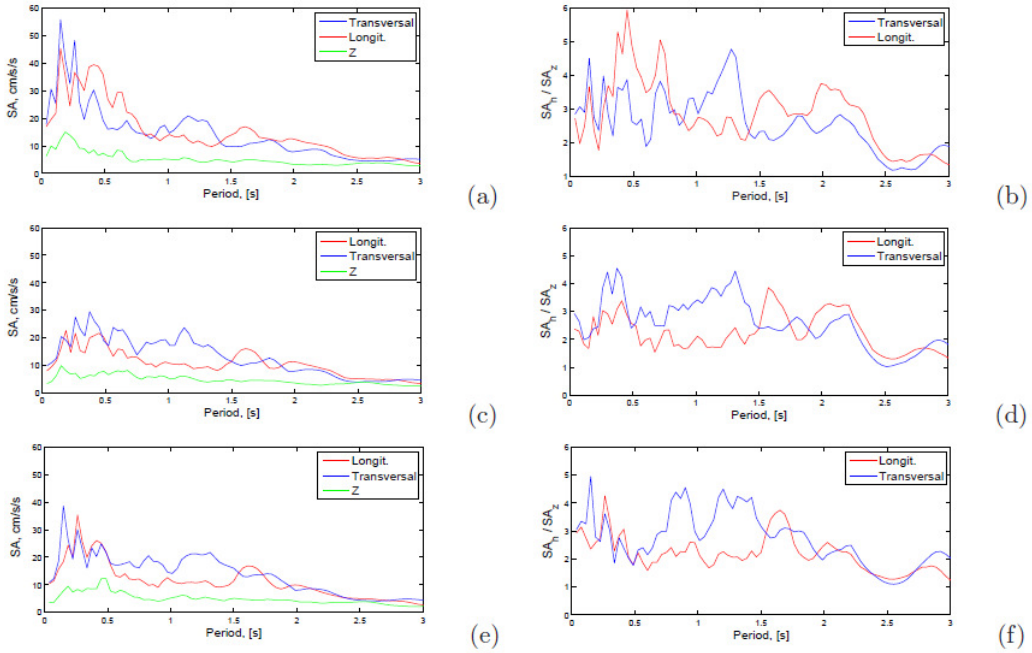

Figure 4. Records of M=6.8 2001 Nisqually earthquake at the location of the critical facility: (a,c,e) response spectra based on triaxial records, ξ=5%, (b,d,f) corresponding H/V response spectra ratios

6. EEWS INSTALLATION AND CONFIGURATION

The on-site EEWS was installed in spring 2009 after several months of testing in the lab environment. The sensor array consists of two instrumented boreholes located at the north and south end of the critical facility, Fig. 5(a). DAQ, communication and power supply units are mounted on the poles next to the protected areas, and are connected into a LAN with a fiber optic cable. All data channels are synchronized using a GPS timing unit installed in the control room, Fig. 5(b). Real-time data from the triaxial sensors of the EEWS array are streamed to the central computer which runs data acquisition software. The main tasks of the software are to: (a) combine all data streams and synchronize them, (b) store data files using a circular buffer, (c) detect the presence of a potential seismic event using a robust pre-triggering algorithm, (d) pass the message about pre-triggered event to the P-wave detection module. The main analysis is done

by the P-wave detection software, which is configured to match the parameters of an expected seismic event. These parameters and the triggering mechanism are described in the next section. The central computer can be accessed via Internet for data download, software updates, or periodic status checks.

(a) (b)

Figure 5. (a) Sensor area of the EEWS, (b) rack-mounted equipment in the control room

Physical configuration of the EEWS and its software architecture include multiple redundancies that decrease the probability of a false alarm. The system is capable of operating if a subset of the sensors fails, if a traffic accident or local industrial sources generate a localized event, the power grid goes down or the Internet connection is not available. System reliability analysis was employed to minimize the risk of a failure and increase the robustness of design.

EEWS is connected to the local shutdown system which operates in an automatic mode. This direct link to the recipient facility maximizes efficiency of the EEWS and increases the warning time. The operator in the control room has the ability to monitor the status of the system which is visualized on the P-wave software GUI. The maintenance plan of the EEWS includes yearly end-to-end tests, a notification procedure in case of a seismic event, and specifies hardware and software replacement intervals. Since DAQ units and the central computer are on the LAN, the system can operate completely without the Internet, which usually becomes unstable immediately after a strong earthquake. All these measures in combination contributed to a successful operation of the EEWS since its installation in 2009.

7. TRIGGERING ALGORITHM

The EEWS system includes 2 borehole strings with 4 triaxial sensors each. A total of 8 sensors located at different depths provide 24 channels of real-time data.

The basic steps of the triggering algorithm are as follows:
(1) Non-recursive FIR band pass filter is applied to each channel y_i:

$$v_{ij} = \sum_{k=1}^{n} c_k y_{i-k,j} \tag{7.1}$$

Coefficients c_k are computed outside of the real-time computations to reduce the computation cost.

(2) Envelope function q_{ij} is computed (Cramer and Leadbetter 1967).

(3) Peak values of q_{ij} are compared with the threshold level.

(4) STA/LTA algorithm (Allen 1978) on the envelope function produces r_{ij} . If $r_{ij} > R$, event is detected at time t_i* for each channel of 8 sensors.

(5) Extract portion of signal $\mathbf{P}_{k\times3}$ that includes the first-motion P-wave from each triaxial record, which corresponds to the time frame $t_p = [t_i^* - \Delta t_1;\ t_i^* + \Delta t_2]$.

(6) Since the source direction is not known, polarization analysis of the seismic wave can be done with the Karhunen-Loéve transform, KLT (Zaicenco et al. 2010), which treats the stochastic process as a combination of the orthogonal functions, and the expansion basis depends on the process itself. We apply discrete KLT to covariance matrix of $\mathbf{P}_{k\times3}$:

$$\Sigma = \mathrm{cov}(\mathbf{P}_i) = \mathbf{QRQ}^T \tag{7.2}$$

Compute normalized variances:

$$w_i = \frac{\mathrm{var}(\mathbf{Y}_i)}{\max(\mathrm{var}(\mathbf{Y}_i))} \tag{7.3}$$

and characterize the polarization properties of the signal.

(7) If k out of 8 sensors exceed threshold polarization and peak levels on k sensors out of 8 are greater than triggering level, the detected event is confirmed as a P-wave.

This triggering algorithm is implemented in real-time P-wave detection software running on a central computer in the control room.

8. SEVERAL EARTHQUAKES RECORDED BY THE EEWS

Hereafter, several significant seismic events recorded by the EEWS during 2009-2011 are presented, Table 8.1, Fig. 1(b). In spite of the differences in the magnitude, these earthquakes resulted in similar PGV at the site, due to different hypocentral distances. The frequency content varied mainly due to the magnitude size.

Table 8.1. Parameters of the earthquakes recorded by the EEWS

Event date [yyyy/mm/dd]	Event time, UTC	Lat. [deg N]	Lon. [deg W]	Magnitude	P-S difference [s]	Focal depth	Hypoc. Dist. [km]	PGV*, Horiz./Vert. [10^{-6} cm/s]
2009/11/17	15:30:46	52.15	-131.38	6.6	≈70	11.6	≈700	1.3/1.1
2011/02/15	14:47:40	48.89	-123.49	2.9	≈6	18	≈45	1.8/0.1
2011/09/09	19:41:34	49.49	-126.97	6.4	≈30	23	≈285	5.9/2.6

*recorded at the bottom sensor

Fig. 6 shows time histories of horizontal components of these records and corresponding normalized time-frequency distributions. These plots indicate that soft soils with a thickness of almost 300 m respond close to their dominant natural frequency T_0≈0.5 Hz during larger-magnitude events. The long duration of this response indicates the presence of a large sedimentary basin with relatively low damping. This corresponds well with the H/V spectral ratios from Nisqually earthquake in Fig.4 (b,d,f), and the known geological structure of the Fraser River delta. The identified natural period of the soil is also confirmed by H/V spectral ratios for M=6.4 2011 seismic event, Fig. 7.

These findings, together with the liquefaction risk assessment of the site, suggest that a regional large-magnitude event will pose a great risk for the normal operation of the critical facility, and the on-site EEWS is a necessary tool to minimize this risk.

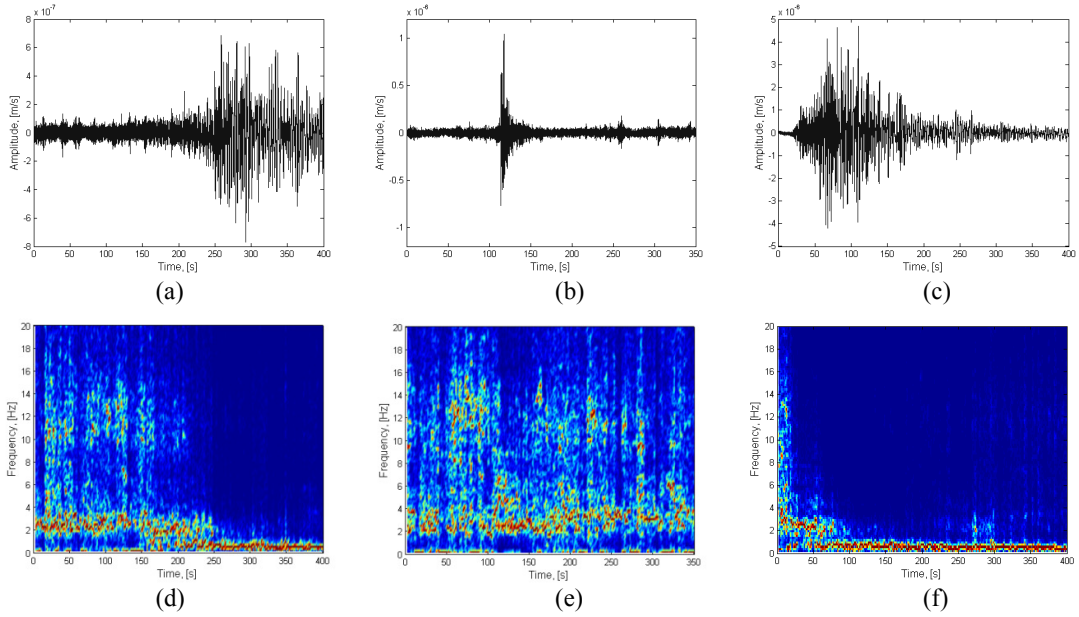

Figure 6. Horizontal components of the recorded earthquakes: (a) 2009/11/17 M=6.6. Time axis starts at 15:30:00 UTC, (b) 2011/02/15 M=2.9. Time axis starts at 14:46:00 UTC, (c) 2011/09/09 M=6.4. Time axis starts at 19:42:00 UTC. (d,e,f) normalized time-frequency distributions using STFT

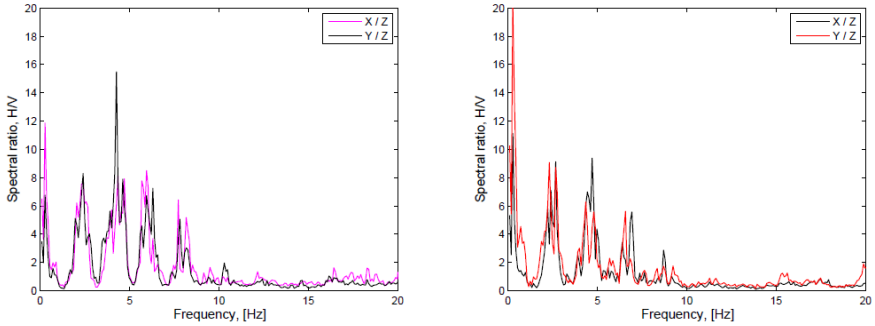

Figure 7. 2011/09/09 M=6.4 seismic event. H/V spectral ratios based on triaxial records: (a) bottom at the north end of the EEWS, (b) bottom at the south end of the EEWS

2011/02/15 magnitude M=2.9 records using triaxial sensors at the north and south ends of the EEWS show frequency and polarization properties of P and S phases, Fig. 8. Singular values of $cov(\mathbf{P}_i)$ and their ratios from Fig. 8(d) indicate strong polarization of body waves. These results are consistent with the records of 2011/09/09 M=6.4 earthquake, Fig. 9, which confirmed that time-dependent frequency content and singular values of $cov(\mathbf{P}_i)$ can be used as one of the main parameters for an efficient P and S-wave discrimination. In this way, the triggering algorithm described in Section 7 has been validated on a small set of recent regional earthquakes.

Time-histories in Fig. 8 and 9 are plotted using local time, i.e. UTC-7 or -8 hrs. Amplitudes of the records are in m/s. Triaxial sensors from the bottom of the instrumented boreholes were used for the analysis due to better SNR. The main source of the noise originates from the highway located in the close proximity of the sensor array.

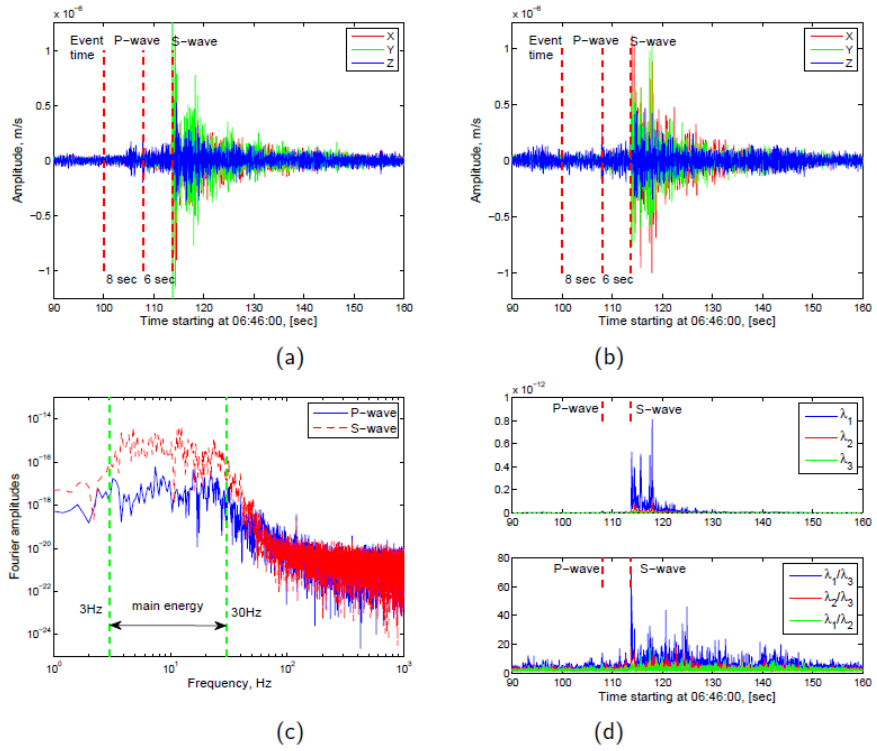

Figure 8. 2011/02/15 M=2.9 record at the bottom sensor, Y component: (a) time history at the north end of the EEWS (local time used), (b) time history at the south end of the EEWS (local time used), (c) frequency content of P and S waves, (d) singular values from Eq.(7.2)

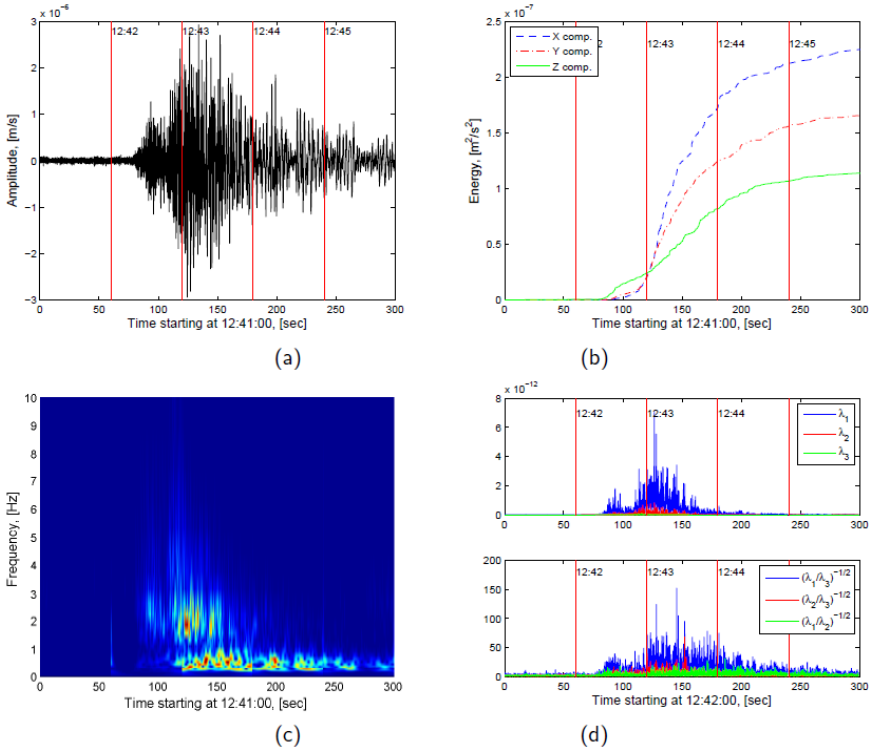

Figure 9. 2011/09/09 M=6.4 record at the bottom sensor: (a) time history (Y comp.), (b) cumulative energy of X, Y and Z components, (c) time-frequency distribution using CWT (Y comp.), (d) singular values from Eq.(7.2)

Findings from the interpretation of the recorded seismic events emphasize the dual use of the on-site EEWS – it reduces the seismic risk for the critical facility on one hand, and, on the other hand, acts as a research tool collecting continuous data on the regional seismicity.

AKCNOWLEDGEMENT

Administrative support provided by the BC Ministry of Transportation is highly appreciated. Records of Nisqually earthquake for the preliminary study in 2009 were kindly provided by Department of Civil Engineering, University of British Columbia, and by the Geological Survey of Canada, Pacific Geoscience Centre.

REFERENCES

Allen, R.M. (1978). Automatic earthquake recognition and timing from single traces. *Bull. Seism. Soc. Am.* **68:5**, 1521-1532.

Atwater, T. (1970). Implications of plate tectonics for the Cenozoic tectonic evolution of western North America, *Geological Society of America Bulletin*. **81**, 3513-3536.

Balfour, N. (2011). Sources of Seismic Hazard in British Columbia: What Controls Earthquakes in the Crust? *PhD dissertation*, the School of Earth and Ocean Sciences, University of Victoria

Cassidy, J., Rogers, G. (1999). Seismic site response in the greater Vancouver, British Columbia, area: spectral ratios from moderate earthquakes, *Can Jeotech. J.*, **36**: 195-209.

Cassidy, J., Rogers, G. and Waldhauser, F. (2000). Characterization of active faulting beneath the Strait of Georgia, British Columbia, *Bulletin of the Seismological Society of America,* **90(5)**: 1188-1199.

Cramer, H. and Leadbetter, M.R. (1967). Stationary and related stochastic processes, *Wiley*, New York

Goldfinger, C., Grijalva, K., Burgmann, R., Morey, A. E., Johnson, J. E., Nelson, C. H., Gutierrez-Pastor, J., Ericsson, A., Karabanov, E., Chaytor, J. D., Patton, J. and Gracia, E. (2008). Late Holocene Rupture of the Northern San Andreas Fault and Possible Stress Linkage to the Cascadia Subduction Zone, *Bulletin of the Seismological Society of America,* **98(2)**: 861-889.

Hyndman, R., Yorath, C., Clowes, R. and Davis, E. E. (1990). The northern Cascadia subduction zone at Vancouver Island: seismic structure and tectonic history, *Canadian Journal of Earth Science*, **27**, 313-329.

Jun Saita, Tsutomu Sato, Yutaka Nakamura. (2008). What is the Useful Application of the Earthquake Early Warning System?, *14th WCEE*, Beijing, China, Oct 12-17.

Kanamori, H., (2005). Real time seismology and earthquake damage mitigation, *Ann. Rev. Earth Planet Sci.*, **33(1)**, 195–214.

Onur, T., Ventura, C., Tao, S. (2001). Strong Motion Records from the February 28, 2001 Nisqually Earthquake Recorded by Three Structural Arrays in BC, Report EQ 01-02, *UBC Earthquake Engineering Research Lab*.

Riddihough, R. (1984). Recent movements of the Juan de Fuca plate system, *Journal of Geophysical Research*, **89(B8)**: 6980-6994.

Rogers, G.C. (1998). Earthquakes and earthquake hazard in the Vancouver area. Clague JJ, Luternauer JL, Mosher DC, Editors. Geology and natural hazards of the Fraser River delta, British Columbia. *GSC Bulletin*, **525**: 17-25.

Seed, H.B., Lysmer, J., and Schnabel, P.B. (1992). SHAKE-91: Equivalent Linear Seismic Response Analysis of Horizontally Layered Soil Deposits, Department of Civil Engineering, University of California, Berkeley.

Wu, Y.M., and Kanamori, H. (2008). Development of an Earthquake Early Warning System Using Real-Time Strong Motion Signals. *Sensors*, **8**:1-9.

Zaicenco A., Alkaz V. (2008). Numerical solution of an elastic wave equation using the spectral method, In: Harmonization of Seismic Hazard in Vrancea Zone, Editors: Zaicenco A., Craifaleanu I., Paskaleva I., Springer, *NATO Science for Peace and Security Series C: Environmental Security*, pp.319-327

Zaicenco, A., Huffman, S., Weir-Jones, I. (2010). Seismic P-wave polarization in the context of on-site early warning system. *5th Intl. Conf. on Recent Advances in Geotech. Eq. Eng. And Soil Dyn*., San Diego, CA, paper #3.12a.

Zaicenco, A., Weir-Jones, I. (2011). Elastic wave polarization using EMD vs. Fourier and wavelet basis. *SEG Expanded abstracts*, San Antonio, Sept 18-23, **30**:4388-4392.

Zollo, A., Amoroso, O., Lancieri, M., Wu, Y.-M. and Kanamori, H. (2010). A threshold-based earthquake early warning using dense accelerometer networks, *Geophys. J. Int.*, **183**: 963-974.